ARL-TR-7327 • JUNE 2015

US Army Research Laboratory

Computational Predictions of Rear Surface Velocities for Metal Plates under Ballistic Impact

by Robert Doney and Joel Stewart

NOTICES

Disclaimers

The findings in this report are not to be construed as an official Department of the Army position unless so designated by other authorized documents.

Citation of manufacturer's or trade names does not constitute an official endorsement or approval of the use thereof.

Destroy this report when it is no longer needed. Do not return it to the originator.

ARL-TR-7327 ● JUNE 2015

US Army Research Laboratory

Computational Predictions of Rear Surface Velocities for Metal Plates under Ballistic Impact

by Robert Doney and Joel Stewart
Weapons and Materials Research Directorate, ARL

REPORT DOCUMENTATION PAGE

Form Approved
OMB No. 0704-0188

1. REPORT DATE *(DD-MM-YYYY)*	2. REPORT TYPE	3. DATES COVERED (From - To)
June 2015	Final	January 2014–May 2015

4. TITLE AND SUBTITLE
Computational Predictions of Rear Surface Velocities for Metal Plates under Ballistic Impact

5a. CONTRACT NUMBER

5b. GRANT NUMBER

5c. PROGRAM ELEMENT NUMBER

6. AUTHOR(S)
Robert Doney and Joel Stewart

5d. PROJECT NUMBER
AH80

5e. TASK NUMBER

5f. WORK UNIT NUMBER

7. PERFORMING ORGANIZATION NAME(S) AND ADDRESS(ES)
U.S. Army Research Laboratory
ATTN: RDRL-WMP-D
Aberdeen Proving Ground, MD 21005-5066

8. PERFORMING ORGANIZATION REPORT NUMBER
ARL-TR-7327

9. SPONSORING/MONITORING AGENCY NAME(S) AND ADDRESS(ES)

10. SPONSOR/MONITOR'S ACRONYM(S)

11. SPONSOR/MONITOR'S REPORT NUMBER(S)

12. DISTRIBUTION/AVAILABILITY STATEMENT
Approved for public release; distribution is unlimited.

13. SUPPLEMENTARY NOTES

14. ABSTRACT
We are interested in quantifying the rear surface (leading-edge) velocities of a series of metal plates as a function of their displacement for impactor diameter, d, and plate thickness, t, such that their ratio, $d/t = \{0.5, 1, 2\}$. Two different plate thicknesses—3.175 and 6.35 mm (1/8 and 1/4-inch, respectively)—are investigated along with 2 different impactor velocities, $v = \{2.3, 8.0\}$ mm/μs. Lastly we investigate these parameters for several common armor materials: rolled homogeneous armor, Ti_6Al_4V, and aluminum 6061-T6. There are a variety of applications for which this information is useful, including material model validation and ballistic limit evaluation.

15. SUBJECT TERMS
ALEGRA, ALE3D, hydrocode, V&V, PDV, velocimetry, plate bulge, free-surface velocity

16. SECURITY CLASSIFICATION OF:			17. LIMITATION OF ABSTRACT	18. NUMBER OF PAGES	19a. NAME OF RESPONSIBLE PERSON
a. REPORT	b. ABSTRACT	c. THIS PAGE			Robert Doney
Unclassified	Unclassified	Unclassified	UU	40	19b. TELEPHONE NUMBER (Include area code) 410-278-7309

Contents

List of Figures

Acknowledgments

We wish to thank Dr Bob Frey (retired) who was the motivation behind this study. We would also like to thank Drs Daniel Hornbaker and James Cazamias for their technical review of the report. We would further like to recognize Dr Steve Segletes and Mr Steve Schraml for LaTeX templates, environment, and support as well as Mr Langston Willis for editorial support. This work was supported in part by a grant of computer time from the Department of Defense (DOD) High Performance Computing Modernization Program at the US Army Research Laboratory, US Army Engineer Research and Development Center, and the Navy DOD Supercomputing Resource Centers.

INTENTIONALLY LEFT BLANK.

1. Introduction

We are interested in temporally and spatially resolving the rear surface velocity of a plate under ballistic impact as a function of materials, impact velocity, and the ratio of plate thickness to impactor diameter. There are a variety of applications for which these details are useful: material model validation, ballistic limit (V_{50}) characterization, and mechanics of layered systems, for example.

Rapacki[1] used free-surface bulging to quantify the remaining armor value of rolled homogeneous armor (RHA). Most previous work however has been related to developing or advancing analytic penetration models. The Walker-Anderson[2] model, which describes long-rod penetrators into semi-inifinite targets, is of particular note. However, it is only applicable until the targets' rear surface affects the penetration process. Ravid et al.[3] extended the model by accounting for target bulging and failure. Separately, Walker[4] derived a velocity field for the back surface bulge to augment their original model. Chocron et al.[5] also extended the Walker-Anderson model to account for different failure criteria—in part to accurately capture the ballistic limit for several targets.

We proceed generating predictive data without the benefit of experiments. While we have attempted to use photon Doppler velocimetry to measure rear surface velocity as the plates deform, results to date have not generated meaningful data (2015 personal communication between M Zellner and R Doney; unreferenced). Target surfaces need to be polished, otherwise debris launched from the rear surface scatters laser light. However, when polishing the surface, specular reflections off of the expanding hemisphere also scatters photons. In both cases an insufficient amount of light is returned to the detectors.

The scope of this effort is to use numerical simulations to quantify the rear surface (leading-edge) velocities of a series of metal plates as a function of their displacement (out to 8 mm) for impactor diameter, d, and plate thickness, t, such that their ratio, $d/t = \{0.5, 1, 2\}$. Two different plate thicknesses—3.175 and 6.35 mm (1/8 and 1/4-inch, respectively)—will be investigated along with 2 different impactor velocities, $v = \{2.3, 8.0\}$ mm/μs. Lastly we investigate these parameters for several common armor materials: RHA, Ti_6Al_4V (Ti64), and aluminum 6061-T6 (Al-6061).

2. Computational Setup

For these 2-dimensional axisymmetric simulations, we use the December 2013 and June 2014 releases of ALEGRA[6] as well as the July 2013 release of ALE3D (4.20).[7] There was no visible difference between the ALEGRA versions although a small performance increase was noted in the 2014 version. ALEGRA calculations were performed in an Eulerian frame while the ALE3D calculations used an arbitrary Lagrangian Eulerian formulation to weight the computational domain toward regions of interest. We are interested in how the responses vary for some cases between the codes, given the different methods they use and their utility in the ballistics and hypervelocity research community. Appendix A compares results between the codes. For the cases compared, we found no significant difference and we proceed using ALEGRA.

2.1 Problem Setup

Figure 1 (not to scale) sketches an example problem where an improvised explosive device surrogate penetrator is modeled as solid copper—but softened with an elevated uniform temperature of 900 K and scaled density—impacts targets of various configurations. Target thicknesses were selected based on their commonality in impact studies. For this effort we are only looking at normal impacts. In the hypervelocity regime, material strength becomes a negligible factor, and materials can be treated hydrodynamically. Codes should manage this self-consistently without the user explicitly modeling material without strength. Here we consider hypervelocity to be anything greater than 6 mm/μs.

To obtain the rear surface velocity of the leading edge, we use a Lagrangian tracer particle, constrained to move along z only, to record the velocity and position. Additionally, its placement with respect to the plate's rear surface is important. If it is too close to the edge it could encounter mixed cells frequently. Mixed cells average quantities which can then affect velocity measurement. If it is too deep inside the plate, it may not adequately represent the rear surface. Calculations are terminated after the particle has moved $z = 8$ mm from its initial position. In this study ALEGRA simulations only use a void insertion model to remove material when the tensile pressure exceeds some value. In general these were drawn from the `PMIN (JFPF0)` values documented as part of the Johnson-Cook (JC) failure model.

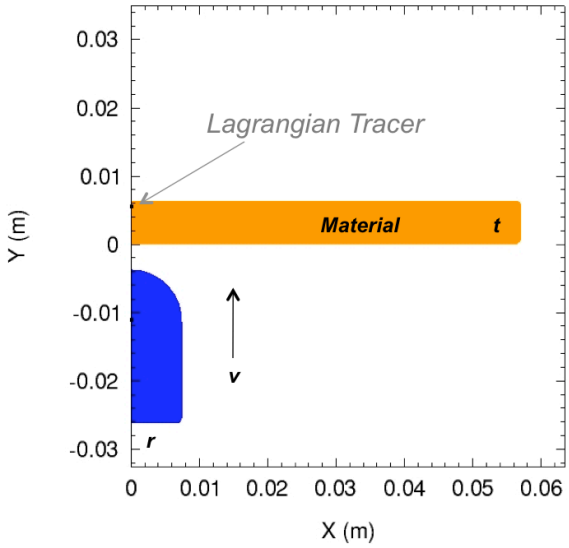

Fig. 1 Typical problem setup

Impactor length, L, is 25.4 mm (1 inch) plus the radius of the adjusted hemispherical nose (which is based on the changing values of the impactor diameter); therefore L/t is always greater than 3 (2014 personal communication between R Frey and R Doney; unreferenced). The velocities were selected based on ballistic regimes of interest: e.g, hydrodynamic transition (around 2–3 mm/μs) and hypervelocity. For the latter, we simply scale up the velocity without changing the threat morphology or material state.

Temporal resolution on the tracer data is 0.025 μs. For a threat moving at 8 mm/μs and 2.3 mm/μs this corresponds to a spatial resolution of 0.2 and 0.058 mm, respectively.

2.2 Material Models

Each material can be modified via its equation of state or constitutive model using any of the many parameters that define it. Unless otherwise noted, in this report we use the default values for each material in a given model. Those values were selected based on early characterization and published work.[8,9]

Appropriateness of material models in penetration metrics has been an ongoing challenge and are not necessarily well characterized. For example, Schraml[10] performed CTH and ALE3D simulations of tungsten rods impacting RHA targets by varying the JC strength parameters of both materials. When Schraml compared re-

sults with experimental data, he found that for a penetration depth to rod length ratio, $P/L = 5$, "the computational results do not yield a single set of parameters that provide a best match to the experimental results." It is helpful to investigate changes in using various material models since the researcher has several to choose from and the most appropriate model is not always clear.

An equation of state (EOS), which relates thermodynamic properties such as temperature pressure, volume, or internal energy, typically comes in the form of a data table or an equation. Unfortunately, there are few validation studies for these models to document their robustness. As this report goes to press however, a new study[11] on the quality of the titanium and Ti64 EOS has become available.

For each material, we compare the Mie-Grüneisen (MG)[12] EOS with SESAME.[13] The SESAME model is a tabular EOS and can generally account for a larger range and greater complexity of material response (e.g., phase changes) than can analytical EOS forms such as MG. However, MG was considered applicable since issues such as phase changes were not expected to be common at 2.3 mm/μs. This report focuses on using the JC strength model[9] to describe the evolution of the yield stress; however, we will also compare the JC results with those obtained from using the Zerilli-Armstrong[14] and Steinberg-Guinan-Lund[15,16] strength models. These details are presented in Appendices B (EOS) and C (Constitutive models). In summary, we found no significant difference among the models.

2.3 Mesh Convergence

As with all calculations, one must spatially resolve the smallest length of interest. In our case, that will be the impactor's smallest radius (1/32 inches; 0.8 mm) since we are constraining the plate thickness and varying its ratio with the impactor. Figure 2 illustrates mesh convergence in terms of the number of cells per millimeter. We define convergence as, given an appropriate variable, once its value does not change by more than some user-determined tolerance, e.g. 2%, it is said to have converged. As the figure shows, refining the mesh from 20 to 30 cells per millimeter changes the tracer's spatial position and, hence our measurement accuracy, by only by a few percent. Therefore it is reasonable to consider that the solution has converged using 20 cells per millimeter (roughly 16 cells across the impactor's radius). Larger values begin to greatly increase the cost and size of calculations. However, just because one variable has converged, it does not mean that other relevant variables have.

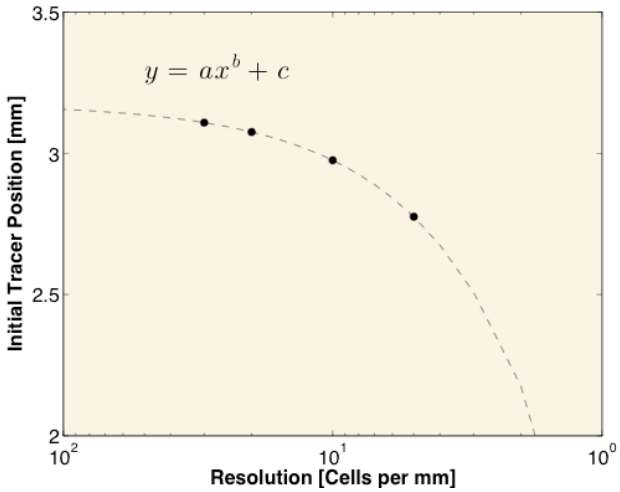

Fig. 2 Mesh convergence of the initial tracer position

Figure 3 illustrates how the resolution (number of cells per millimeter) affects the back surface velocity—our primary metric. The inset in panel (a) represents a zoomed region of the initial expansion. In all cases, the lowest resolution (5 cells per millimeter) was expected to be unacceptable a priori. In panel (a), with a threat diameter of approximately 1.6 mm, resolutions are 8, 16, 32, and 48 cells across the threat diameter (5, 10, 20, and 30 cells per millimeter, respectively). In panel (b), using the same settings with the largest threat diameter of 12.7 mm, resolutions become 63.5, 127, 254, and 381 cells across the threat diameter.

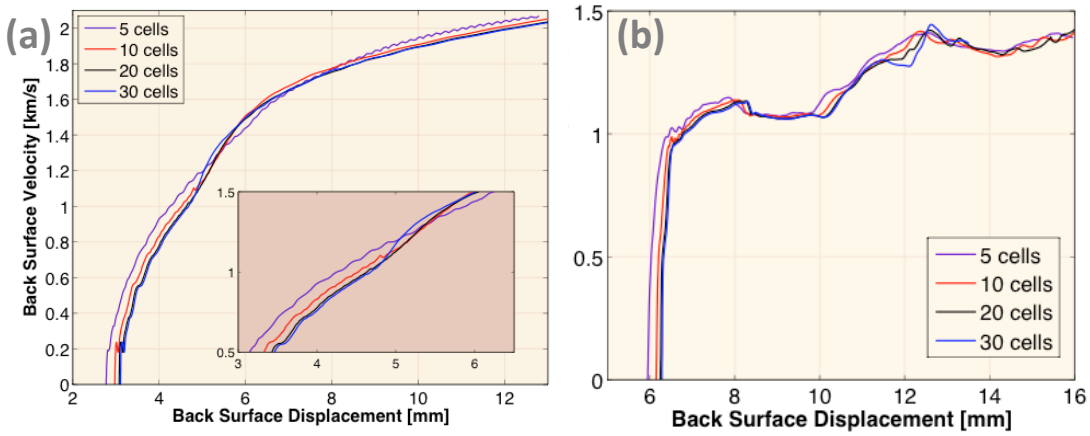

Fig. 3 ALEGRA convergence study: RHA; $v_i = 2.3$ mm/μs; (a) $t = 3.175$ mm, $d/t = 0.5$, $d = 1.5$ mm; (b) $t = 6.35$ mm, $d/t = 2, d = 12.7$ mm

3. Results and Discussion

We expect the shock impedance, $Z = \rho_0 U$, to govern early behavior. Here, ρ_0 is the initial density, and U is the shock velocity. Figure 4(a) shows the ratio of the 3 plate material shock impedances to that of the copper projectile. Physically, shock impedance is the measure of a material's ability to generate pressure under loading conditions.[17]

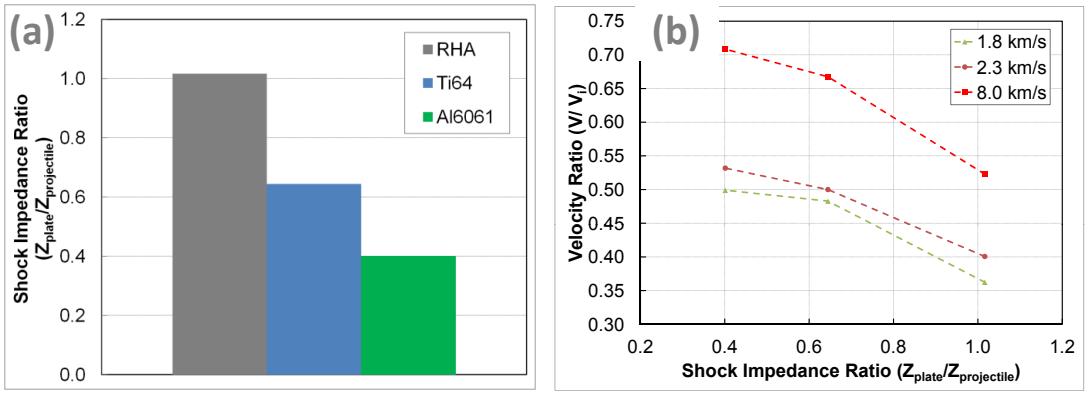

Fig. 4 (a) Ratio of the target material's shock impedance to the shock impedance of the copper projectile and (b) normalized back-surface velocity after a displacement of 2 mm versus shock impedance ratio ($\mathrm{d/t} = $ 1.0, $\mathrm{t} = 6.35$ mm)

Figure 4(b) plots the rear surface velocity normalized by impact velocity of 1/4-inch plates after a displacement of 2 mm and plotted versus the shock impedance ratio. For all impact velocities, the velocity ratio decreases as the shock impedance ratio increases. This trend was generally found to hold across all calculations.

3.1 Constant Material

Figure 5 illustrates the results for RHA. Within each subplot, we see the effects of adjusting d/t—the width of the penetrator with respect to target thickness. At $v = 2.3$ km/s (top row), for both cases the target response transitions from a smooth expansion to ringing and a slower expansion after some initially faster displacement as d/t increases. We also observe the expansion velocity among threat sizes crosses over about 2 mm for the thin plate and 4–5 mm for the larger plate. Put another way, after 2 mm of plate bulge growth for 1/8-inch plates, the expansion velocity of the plate's rear surface is moving at about 1.2 km/s—independent of the penetrator's width (for these select cases). Thereafter, thinner threats lead to an increased expansion velocity over wider threats. This is caused by a greater amount of lo-

calized energy deposition for small d/t—there is less inertia and strength in the increasingly thin, bulging plate to oppose and erode the threat. When going to a thicker plate (upper right panel) that velocity crossover requires a larger displacement and ultimately results in slower expansion velocities. However, the expansion rates caused by threats equal to and greater than the plate thickness ($d/t \geq 1.0$) are roughly equivalent.

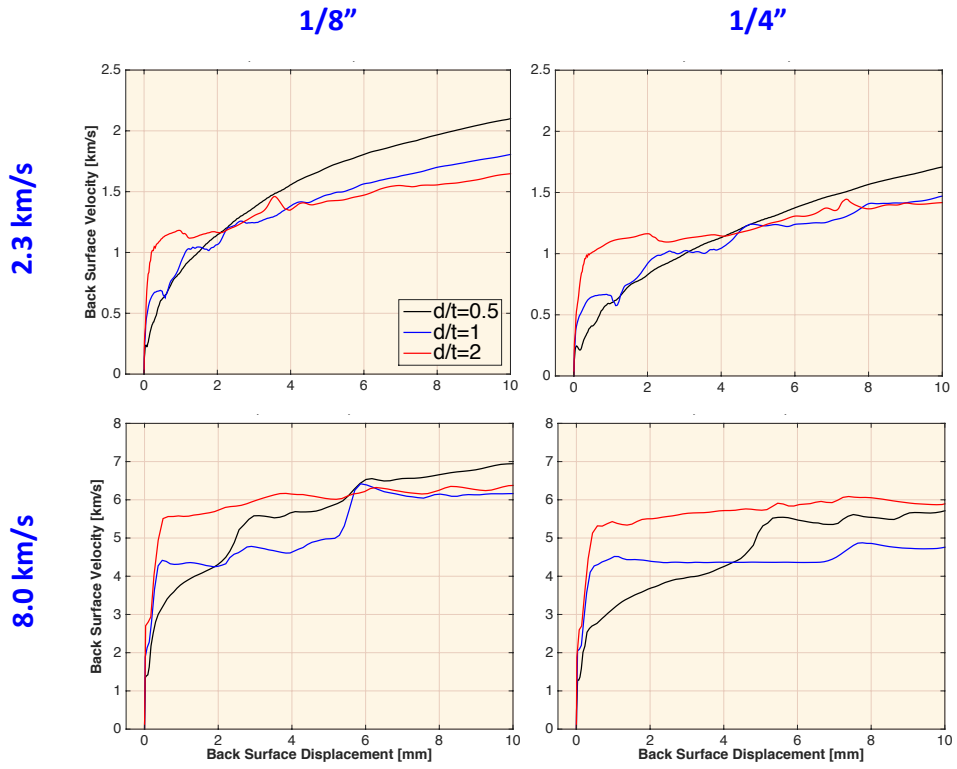

Fig. 5 ALEGRA simulations of RHA

For faster threats into RHA (Fig. 5, bottom row), larger diameter threats permit a higher initial expansion rate of the targets' leading edge. We can better visualize these dynamics for 1/8-inch plates and $d/t = 0.5, 1$. Figure 6 is a composite image for subsequent displacements of 1 mm. The image dump frequency is 100 ns so each image is approximate with respect to the displacement. Note the differences in plate thickness about the penetrator as it deforms.

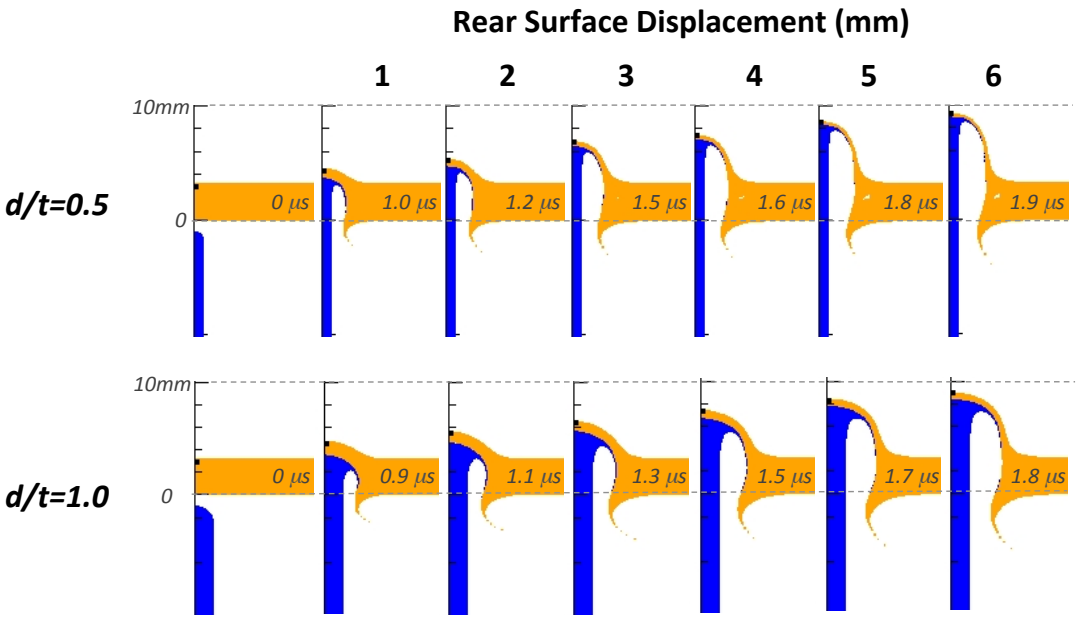

Fig. 6 Spatial display of $\mathrm{v} = 8$ km/s, $\mathrm{d/t} = 0.5, 1$, $\mathrm{t} = 1/8$-inch; cases from Fig. 5 lower-left panel

Ti64 and Al-6061 results are presented in Fig. 7 and Fig. 8, respectively. Results are quite similar; here we discuss the Ti64 data only. In the top row for threats wider than the target thickness ($d/t = 2$), there is a large shock-up in velocity followed by a saturating velocity. A larger threat means more momentum delivered to the target as well as a greater volume of target material that must flow out of the threat's path or fail. With increasingly narrow threats (at 2.3 mm/μs), the expansion is more gradual—again following a power law behavior—and the back surface velocity ultimately surpasses those for the wider threats. This crossover occurs between 2–4 mm for 1/8-inch plates and 4–10 mm for the 1/4-inch plates. Therefore, initially the larger threats deliver greater momentum to the target causing a rapid climb in the rear surface velocity. Inertial effects caused by those larger target areas eventually slow expansion, allowing the more localized (small d/t) interactions to dominate. The transition is more pronounced in the 1/8-inch plates and is evident for all 3 plate materials.

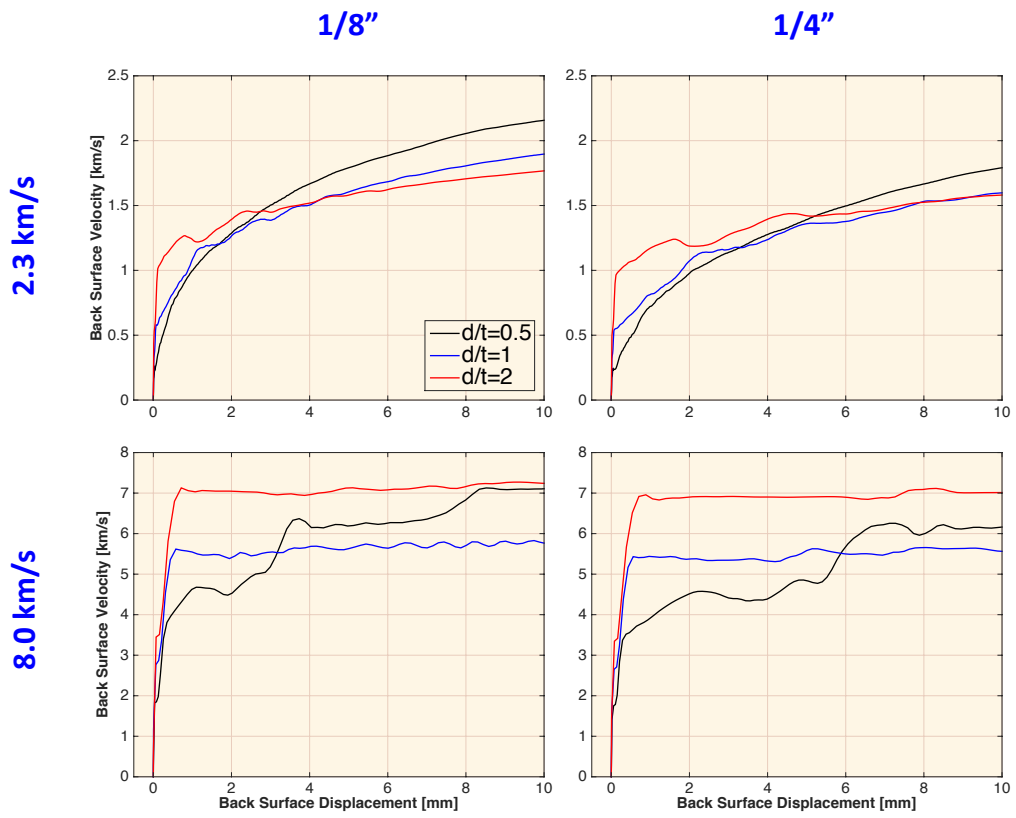

Fig. 7 ALEGRA simulations of Ti64

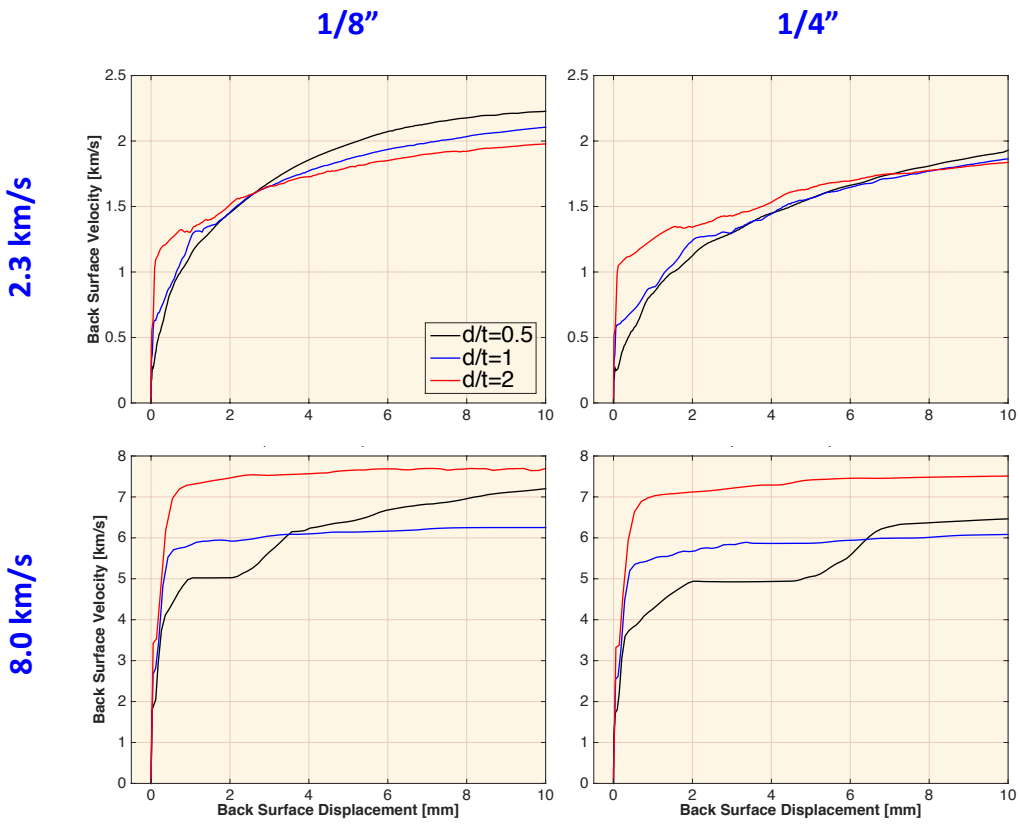

Fig. 8 ALEGRA simulations of Al-6061

3.2 Constant Velocity

Figure 9 and Fig. 10 illustrate results where initial threat velocities are 2.3 and 8.0 mm/μs, respectively. Within each plot, we see the effects of altering target material. In both figures, rows of plots correspond to target plate thickness while columns represent d/t. Recall that for $d/t = 0.5$, the threat diameter, d, is half the plate thickness, t, while for $d/t = 2.0$, the threat diameter is twice the plate thickness. Each plot illustrates the plates' (leading edge) rear surface velocity as a function of its displacement out to 8 mm for RHA, Al-6061, and Ti64.

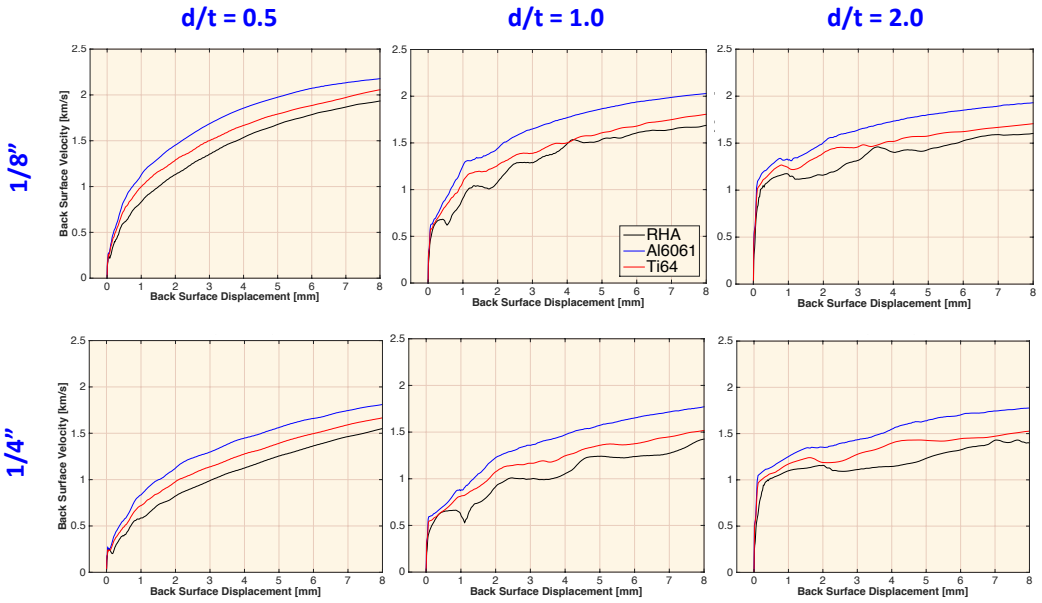

Fig. 9 ALEGRA results for 2.3 mm/μs

In all cases for Fig. 9, Al-6061 has the fastest expansion velocity followed by Ti64 and then RHA. Recall that this is consistent with the shock impedance: the velocity ratio is seen to decrease as the shock impedance ratio increases ($Z_{Al} < Z_{Ti64} < Z_{RHA}$). The leftmost column represents impactors whose diameter is half the plate thickness. For both 1/4- and 1/8-inch plates, there is an immediate jump in rear surface velocity to about $v/10$ and then a smooth increase. After about 2 mm of displacement, there is about a 200 m/s difference between the Al-6061 and Ti64 expansion velocities for 1/8-inch plates. This drops to approximately 125 m/s with the thicker 1/4-inch plates. These differences remain fairly constant during the remaining expansion. Also for the $d/t = 0.5$ cases, the expansion is sufficiently smooth that the data can be described by a simple power law, $V = az^b$, where V is the rear surface velocity and z is the rear surface displacement. Using the curve fitting tool-

box in MATLAB, we find for RHA (left column, black curve) that $V = 0.85z^{0.41}$ for $1/8$-inch plates and $V = 0.6z^{0.46}$ for $1/4$-inch plates. Additional studies can carry this further where a, b become functions of plate material and thickness. As the threat increases in diameter (larger d/t), nonlinearities in the expansion emerge, which are more pronounced for RHA. Strength effects play some role in the bulk response.

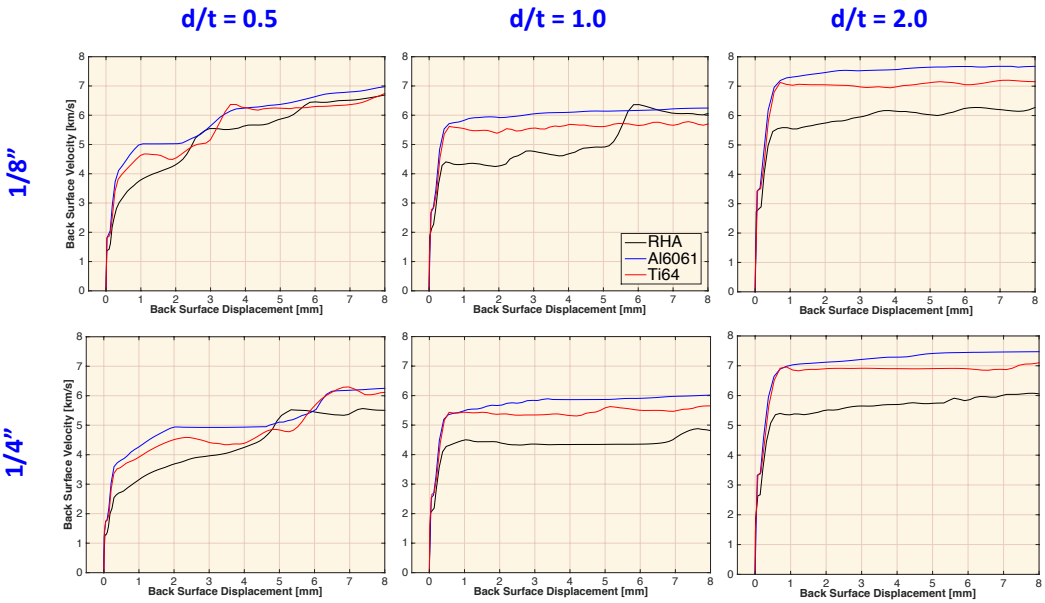

Fig. 10 ALEGRA results for 8.0 mm/μs

As noted already, in each of the 6 plots there is an immediate shock-up in velocity over very short distance. At $d/t = 0.5$, material effects begin playing a role once v =250 m/s. At $d/t = 1.0$ that happens at $v = 500$ m/s, and at $d/t = 2.0$ material effects begin playing a role between 500–1000 m/s. Thus the magnitude of the initial velocity jump in the rear plate scales with d/t linearly.

Figure 10 looks at the hypervelocity regime where most of the interesting behavior is for threat diameters sized at half the plate thickness ($d/t = 0.5$), and where there appears to be competing mechanisms for both plate thicknesses. Again, in all cases there is a 2-phase jump in the plate's rear surface velocity: an initial "fast phase" due to the shock, followed by one where material effects begin shaping the results. This transition increases (somewhat linearly) with d/t but does not change significantly with plate thickness. Most of the remaining data is unremarkable as hydrodynamic behavior allows the penetrator to continue with little disruption.

4. Conclusion

In this report, we used ALEGRA simulations to quantify the rear surface (leading-edge) velocities of a series of metal plates as a function of their displacement for impactor diameter to plate thickness ratios $d/t = \{0.5, 1, 2\}$. Plate thicknesses of 1/8-inch and 1/4-inch were investigated, as were impactor velocities of 2.3 and 8.0 mm/μs. Several common armor materials were utilized for the target: RHA, Ti64, and Al-6061. The primary role of d/t is in energy localization.

In each of the target materials studied, where impactor velocities are 8 mm/μs, there is an interesting crossover in back surface velocity between the $d/t = \{0.5, 1\}$ cases when changing the plate thickness. Specifically, when $d/t = 1.0$ impact 1/8-inch plates—so the penetrator diameter is also approximately 3 mm—there is a rapid acceleration of the target's rear surface velocity to 5.5–6.0 mm/μs for Al-6061 and Ti64 and roughly 4.5 mm/μs for RHA where they remain mostly constant thereafter (with variations for RHA). Thinner threats however, overtake this expansion velocity after the plate has expanded some distance. Simulations suggest that this crossover doubles with plate thickness: from approximately 3 to 6 mm for Al-6061 and Ti64 and 2 to 4 mm for RHA.

Initially the larger threats deliver greater momentum to the target causing a rapid climb in the rear surface velocity. Inertial effects caused by those larger target areas eventually slow expansion, allowing the more localized (small d/t) interactions to dominate. The transition is more pronounced in the thinner 1/8-inch plates and is evident for all 3 plate materials.

Future work should consider the effects of obliquity as well as velocity perturbations about the hydrodynamic transition. We will also continue to resolve ongoing difficulties with collecting photon doppler velocimeter data.

5. References

1. Rapacki EJ. Analysis of terminal metallic armor plate free-surface bulging. Aberdeen Proving Ground (MD): Army Research Laboratory (US); 2008 Oct. Report No.: ARL-RP-231. Also available at http://www.arl.army.mil/www /default.cfm?technical_report=1703.

2. Walker JD, Anderson CE. A time-dependent model for long-rod penetration. International Journal of Impact Engineering. 1995; 16(1): 19–48.

3. Ravid M, Bodner SR, Walker JD, Chocron S, Anderson CE, Riegel JP. Modification of the Walker-Anderson penetration model to include exit failure modes and fragmentation. In: Van Niekerk C, editor. Ballistics '98. Proceedings of the 17th International Symposium on Ballistics Vol. 3; 1998 Mar 23–27; Midrand, South Africa. The Organization. p. 267–274.

4. Walker JD. An analytic velocity field for back surface bulging. In: Reinecke WG, editor. Ballistics '99. Proceedings of the 18th International Symposium on Ballistics; 1999 Nov 15–19; San Antonio, TX. Lancaster (PA): Technomic Pub Co. p. 1239–1246.

5. Chocron S, Anderson CE, Walker JD. A consistent plastic flow approach to model penetration and failure of finite-thickness metallic targets. In: Reinecke WG, editor. Ballistics '99. Proceedings of the 18th International Symposium on Ballistics; 1999 Nov 15–19; San Antonio, TX. Lancaster (PA): Technomic Pub Co. p. 761–768.

6. Robinson AC, Brunner TA, Carroll S, Drake R, Garasi CJ, Gardiner T, Haill T, Heath H, Hensinger D, Labreche D, et al. ALEGRA: An arbitrary Lagrangian-Eulerian multimaterial, multiphysics code. In: Proceedings of the 46th AIAA Aerospace Sciences; 2008 Jan 7–10; Reno, NV. Reston (VA): American Institute of Aeronautics and Astronautics; 2008. p.1235–1274.

7. Nichols A. An arbitrary Lagrange/Eulerian 2D and 3D code system, version 4.20.x, volumes 1 and 2. Livermore (CA): Lawrence Livermore National Laboratories; 2013 Jul. Report No.: LLNL-SM-642812.

8. Gray G, Chen S, Wright W, Lopez M. Constitutive equations for annealed metals under compression at high strain rates and high temperatures. Los Alamos (NM): Los Alamos National Laboratory; 1994. Report No.: LA-12669-MS.

9. Johnson G, Cook W. A constitutive model and data for metals subjected to large strains, high strain rates and high temperatures. In: Proceedings of the 7th International Symposium on Ballistics; 1983 Apr 19–21; The Hague, The Netherlands. p. 541–547.

10. Schraml S. Constitutive model parameter study for armor steel and tungsten alloys. Aberdeen Proving Ground (MD): Army Research Laboratory (US); 2012 Jan. Report No.: ARL-RP-351. Also available at http://www.arl.army.mil/www/default.cfm?technical_report=6328.

11. Mattsson AE, Sanchez J. Equation of state model quality study for Ti and Ti64. Albuquerque (NM): Sandia National Laboratories. 2015 Feb. Report No.: SAND2015-1197.

12. Walsh JM, Rice MH, McQueen RG, Yarger FL. Shock-wave compressions of twenty-seven metals. Equations of state of metals. Physical Review. 1957; 108(2):196–216.

13. Lyon SP, Johnson JD. SESAME: The Los Alamos National Laboratory equation of state database. Los Alamos (NM): Los Alamos National Laboratory; 1992. Report No.: LA-UR-92-3407.

14. Zerilli FJ, Armstrong RW. Dislocation-mechanics-based constitutive relations for material dynamics calculations. Journal of Applied Physics. 1987; 61(5):1816–1825.

15. Steinberg DJ, Lund CM. A constitutive model for strain rates from 10^{-4} to 10^{6} sec^{-1}. Journal of Applied Physics. 1989; 65: 1528.

16. Taylor PA. CTH reference manual: The Steinberg-Guinan-Lund viscoplastic model. Albuquerque (NM): Sandia National Laboratories; 1992. Report No.: SAND92-0716.

17. Stilp AJ, Weber K. Debris clouds behind double-layer targets. International Journal of Impact Engineering 1997; 20(6-10): 765–778.

INTENTIONALLY LEFT BLANK.

Appendix A. Comparison between ALEGRA and ALE3D

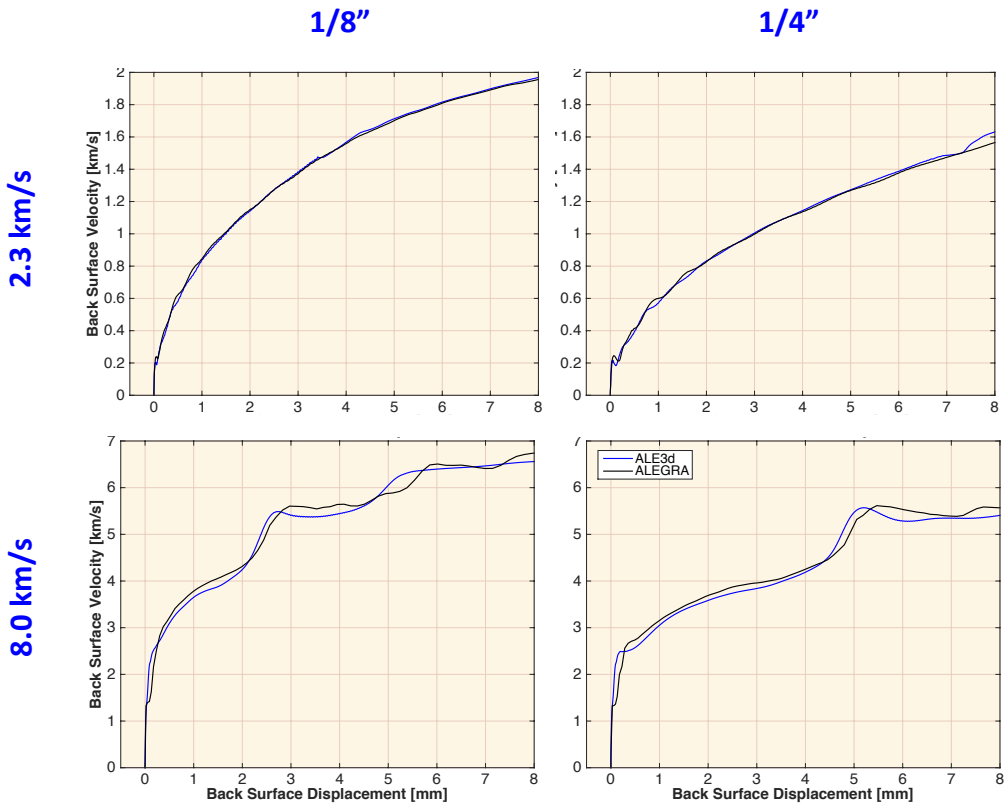

Fig. A-1 Comparison of rolled homogeneous armor between ALEGRA and ALE3D for $\mathbf{d/t = 0.5}$

The qualitative behavior of the ALE3D calculations was found to be quite sensitive to both the pressure relaxation scheme (`presseq`) and the element integration type (`elem_integration`) used. The default values for both `presseq` and `elem_integration` often resulted in oscillatory behavior at lower velocities, especially at later times. It was determined that turning off pressure relaxation (i.e., setting `presseq`=0) tended to minimize the oscillatory behavior. Changing the element integration from the 2-dimensional axisymmetric default of Wilkins (`elem_integration` = 3) to the Flanagan-Belytschko formulation (`elem_integration` = 2) also seemed to minimize the oscillatory behavior, but this setting was not thoroughly investigated. All ALE3D calculations shown in this report used the default of Wilkins for the element integration scheme but turned off the pressure relaxation.

Appendix B. Equations of State

Figure B-1 through Fig. B-4 use prototypical calculations to compare the differences between the Mie-Grüneisen (MG) and SESAME equations of state (EOS) for the relevant materials. In each case we use the Johnson-Cook (JC) strength model with default values from ALEGRA's material library. While the primary data in this report does not consider fracture models, the comparisons below do include default settings of the JC fracture model[1]. Our interest was in observing the increased likelihood for sensitive parameters. In general the differences are only minor (less than 10%) and just a few cases warrant further investigation. We note also that for some cases, there are brief data drops due to the tracer particle passing into cells consisting only of void. Since there is little difference in the results, the data are presented without further analysis. Physical significance of the results are presented in the primary report.

There is not any default MG model specific to rolled homogeneous armor (RHA), although variations on steel are an option. Instead, in Fig. B-4 we look at 2 sets of SESAME parameters tuned for RHA: the default values published by Gray et al.[2] and those reported by Brar et al.[3] Clearly there is substantial agreement between the datasets with the largest deviation (5%–10%) occurring in the upper right panel for 1/8-inch plates after approximately 5 mm of displacement.

[1]Johnson GR, Cook WH. Fracture characteristics of three metals subjected to various strains, strain rates, temperatures and pressures. Engineering Fracture Mechanics. 1985; 21(1): 31-48.

[2]Gray GT, Chen SR, Wright W, Lopez MF. Constitutive equations for annealed metals under compression at high strain rates and high temperatures. Los Alamos (NM): Los Alamos National Laboratory; 1994. Report No. LA-12669-MS.

[3]Brar N, Abfalter G, Brockman R, Poormon, K. Material characterization of RHA, titanium 6-4, Mg-Az31B-O, and Al-SiC MMC 359. Warren (MI): Army Tank Automotive Research, Development, and Engineering Center (US); 2011 Aug. Report No.: UDR-TR-2011-00129.

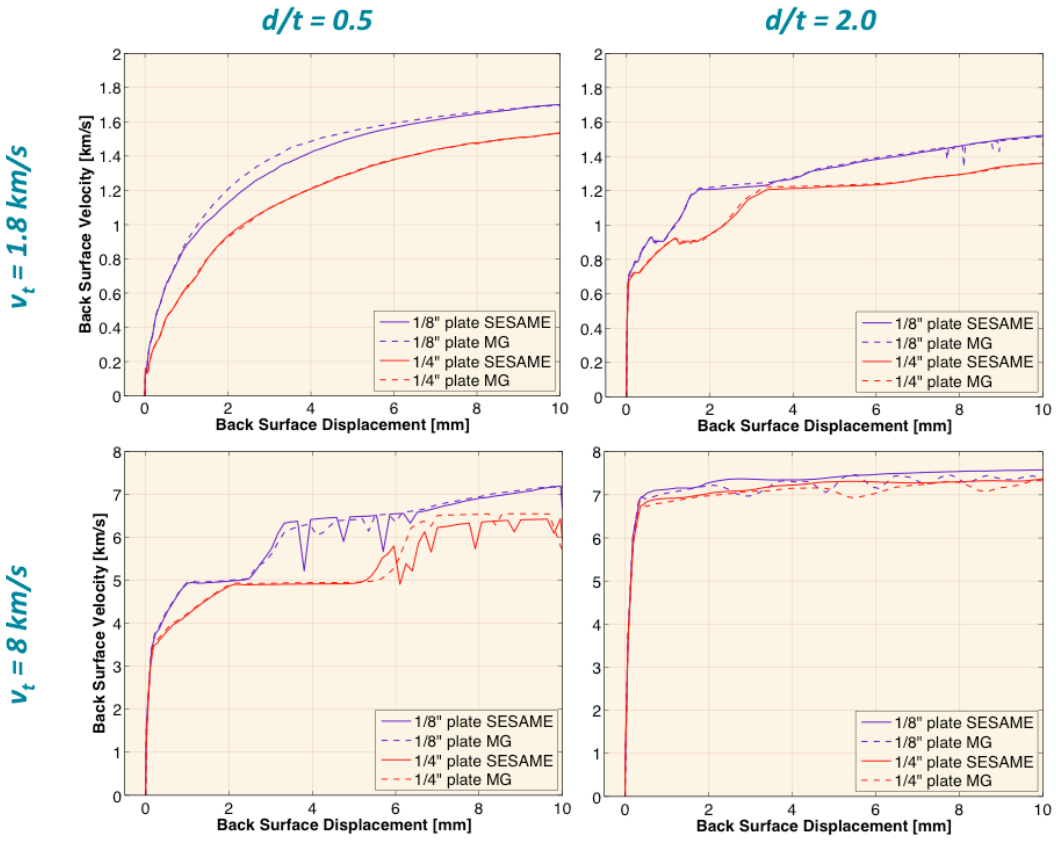

Fig. B-1 SESAME and MG EOS models for Al-6061

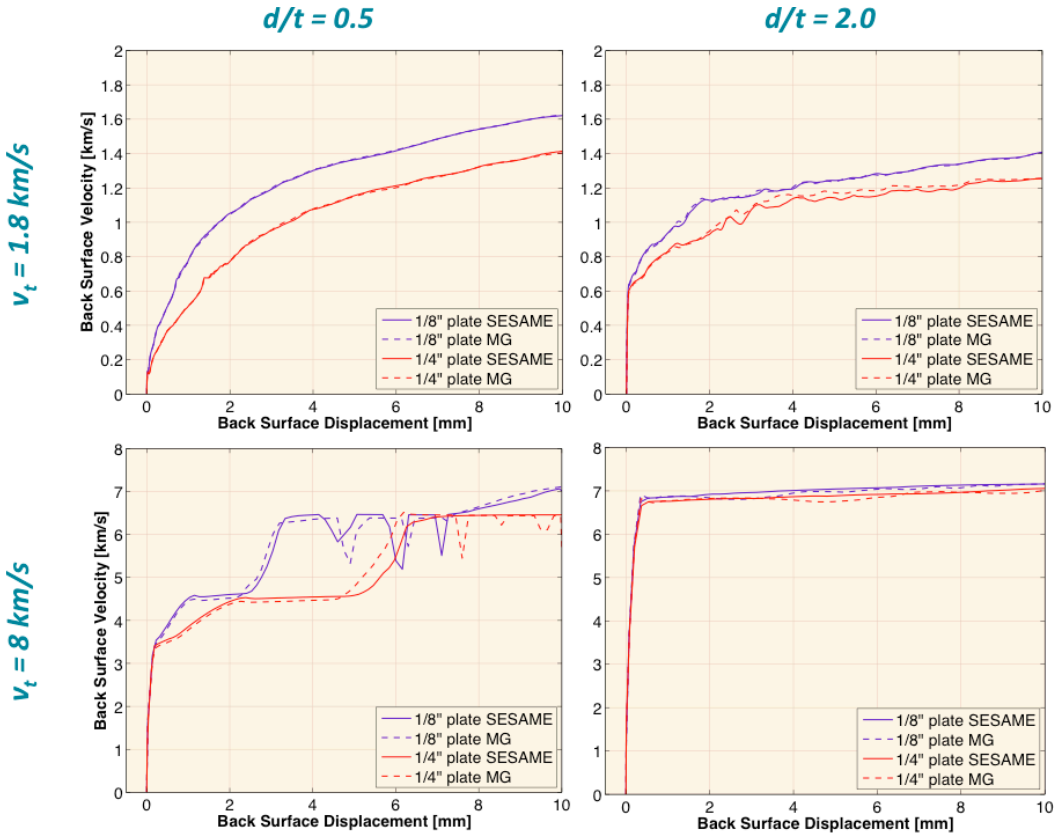

Fig. B-2 SESAME and MG EOS models for Ti64

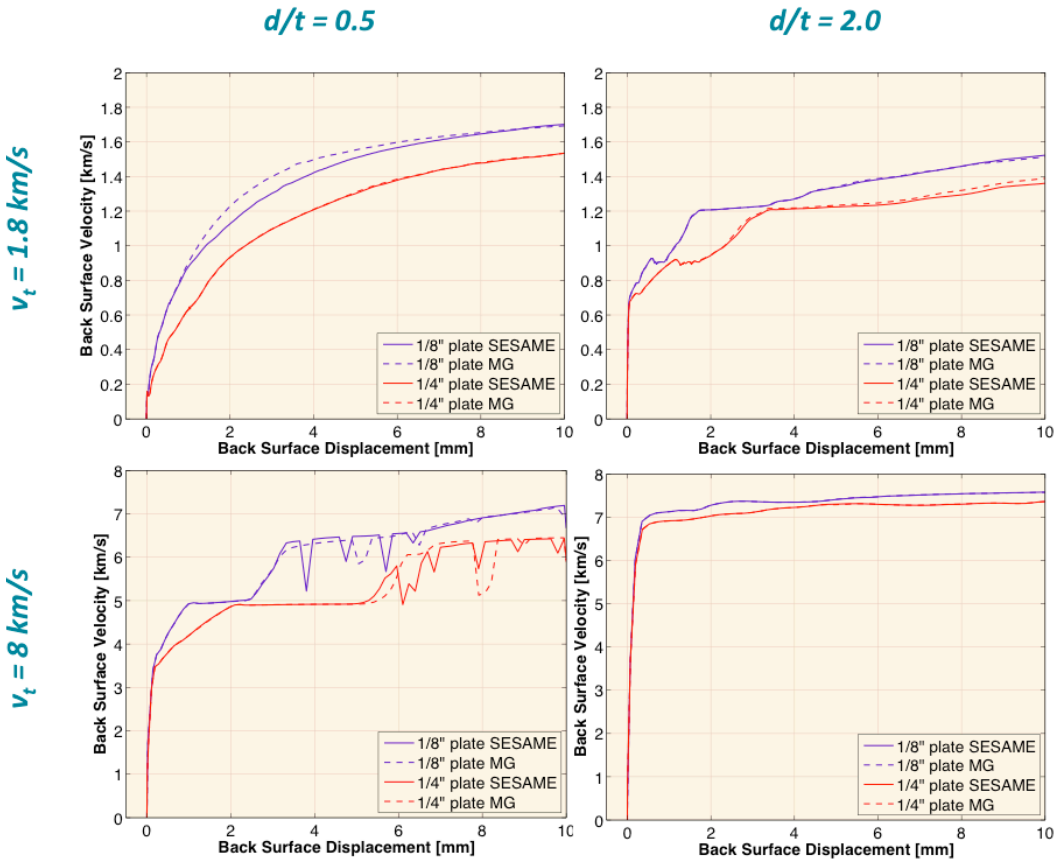

Fig. B-3 SESAME and MG EOS models for Cu

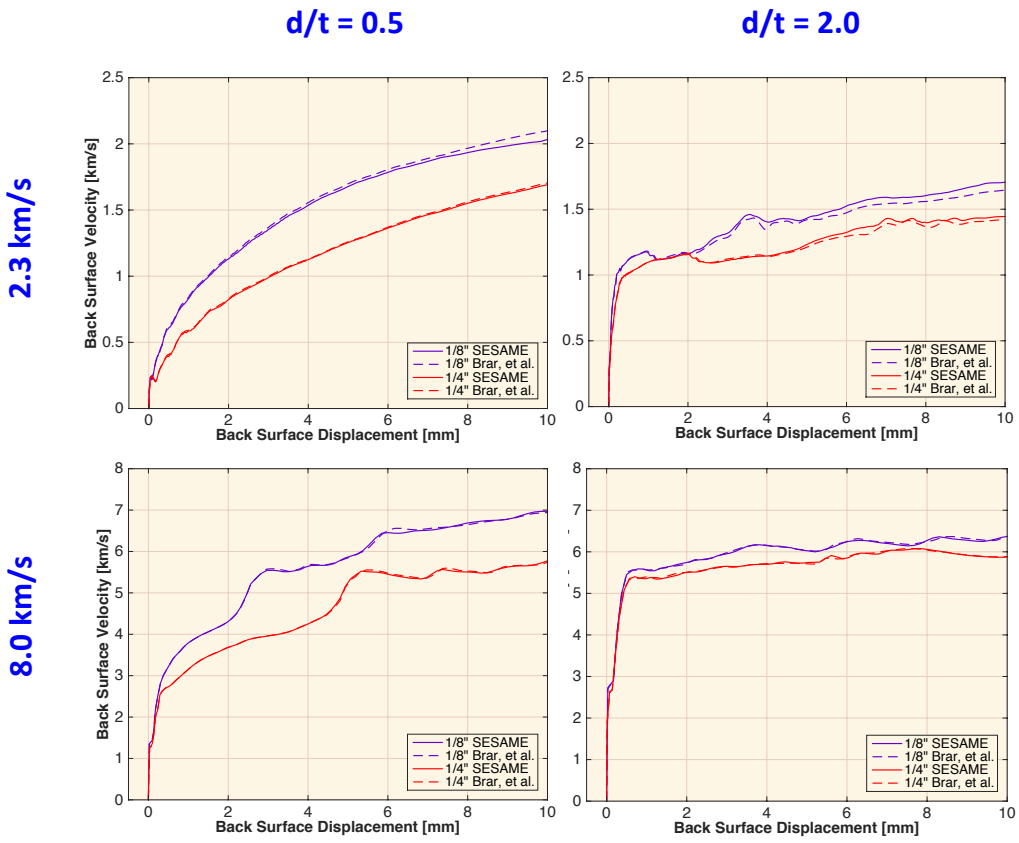

Fig. B-4 Two sets of SESAME EOS parameters for RHA

Appendix C. Constitutive Model

Figure C-1 through Fig. C-4 illustrates the negligible differences between the Zerilli-Armstrong (ZA) and Johnson-Cook (JC) strength models in this study. These represent the default values for both models with the caveat that, for rolled homogeneous armor (RHA) with JC, `AJ0` depends on plate thickness as reported by Meyer and Kleponis[1]. Each simulation uses a SESAME equation of state and JC fracture with a fracture pressure (tension) of 2.5 GPa (2014 personal communication between HW Meyer and R Doney; unreferenced). In our attempts to manage unexpected fracture behavior in the tip of the penetrator in some cases, we increased the magnitude of the fracture pressure to $-1 \cdot 10^{15}$ Pa, thus ignoring tensile failure. However, that introduces about a 10% variation in results at late times.

We repeat a similar set of calculations for aluminum as in the previous section, but in this case there is not a predefined ZA model for Al-6061. Instead we use the default settings for Steinberg-Guinan-Lund (SGL). Since there is little difference in the results, the data is presented without further analysis. Observations are discussed in the main body of the report.

[1]Meyer HW, Kleponis DS. An analysis of parameters for the Johnson-Cook strength model for 2-in thick rolled homogeneous armor. Aberdeen Proving Ground (MD): Army Research Laboratory (US); 2001 Jun. Report No.: ARL-TR-2528.

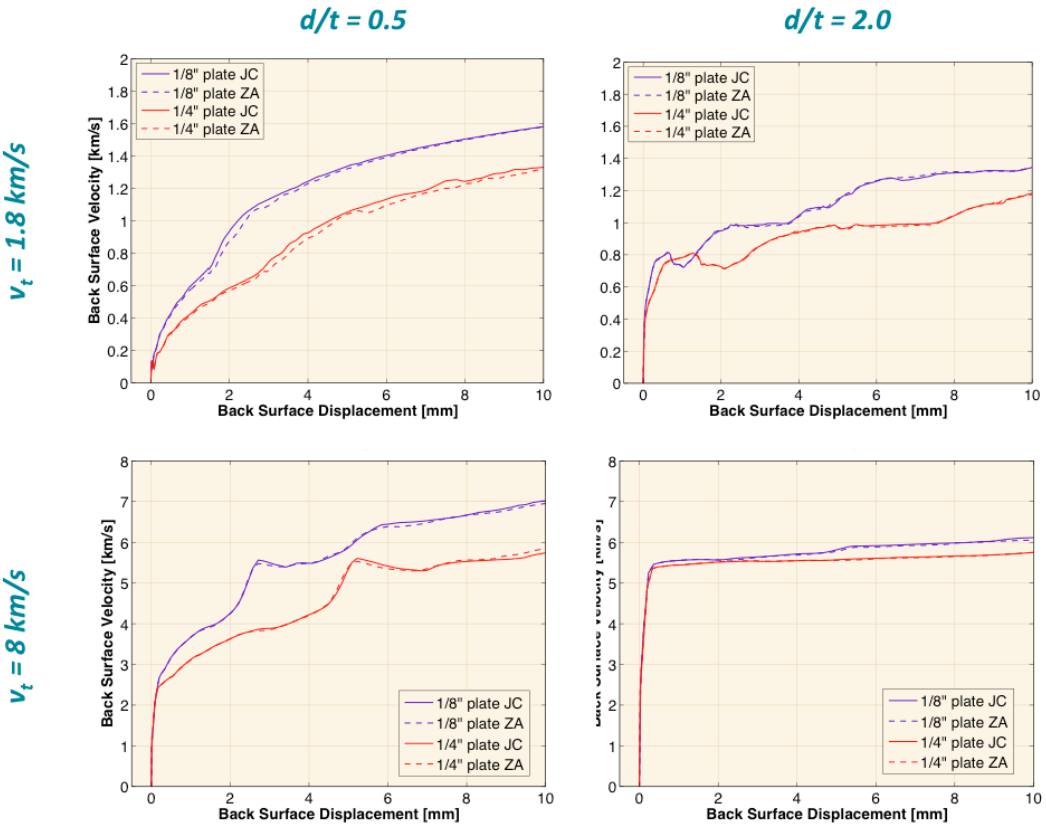

Fig. C-1 JC and ZA strength models for RHA

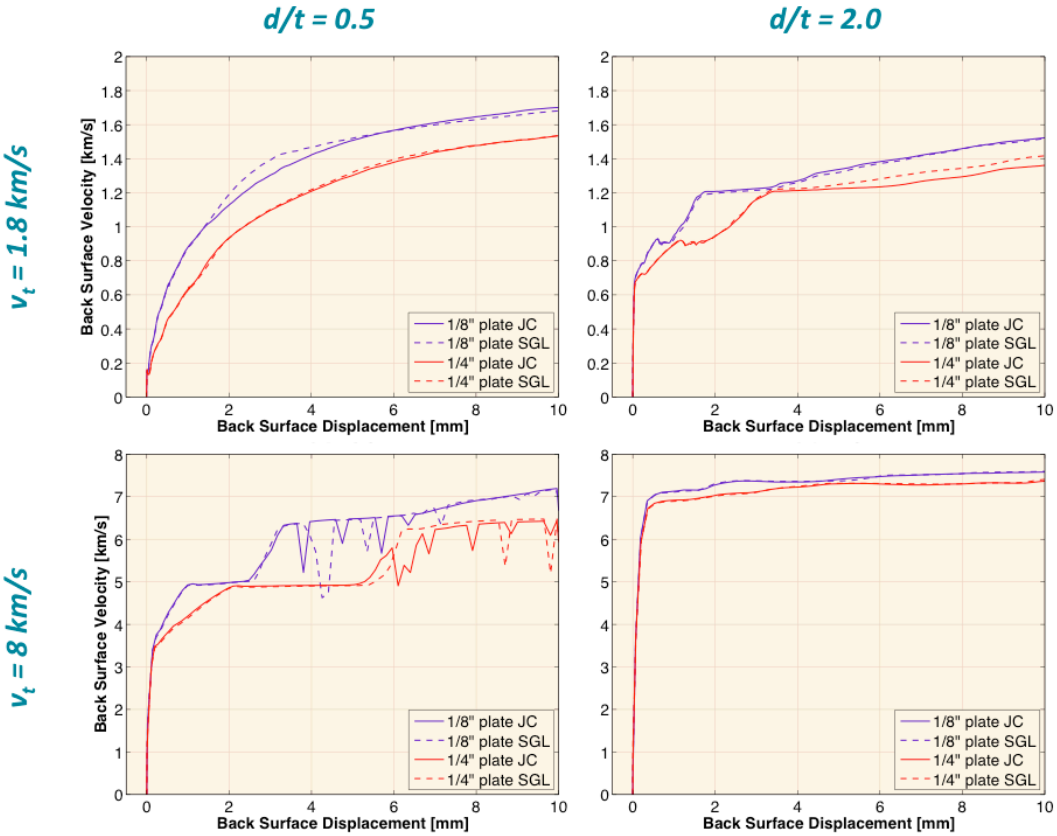

Fig. C-2 JC and SGL strength models for Al-6061

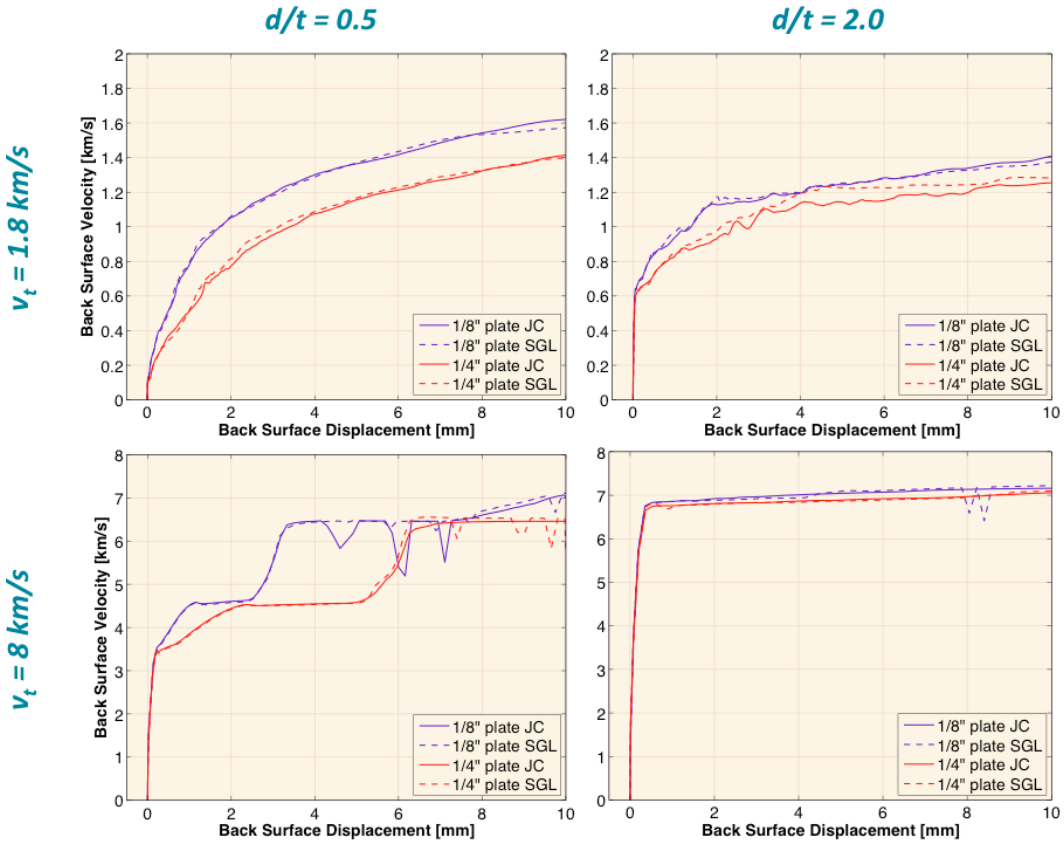

Fig. C-3 JC and SGL strength models for Ti64

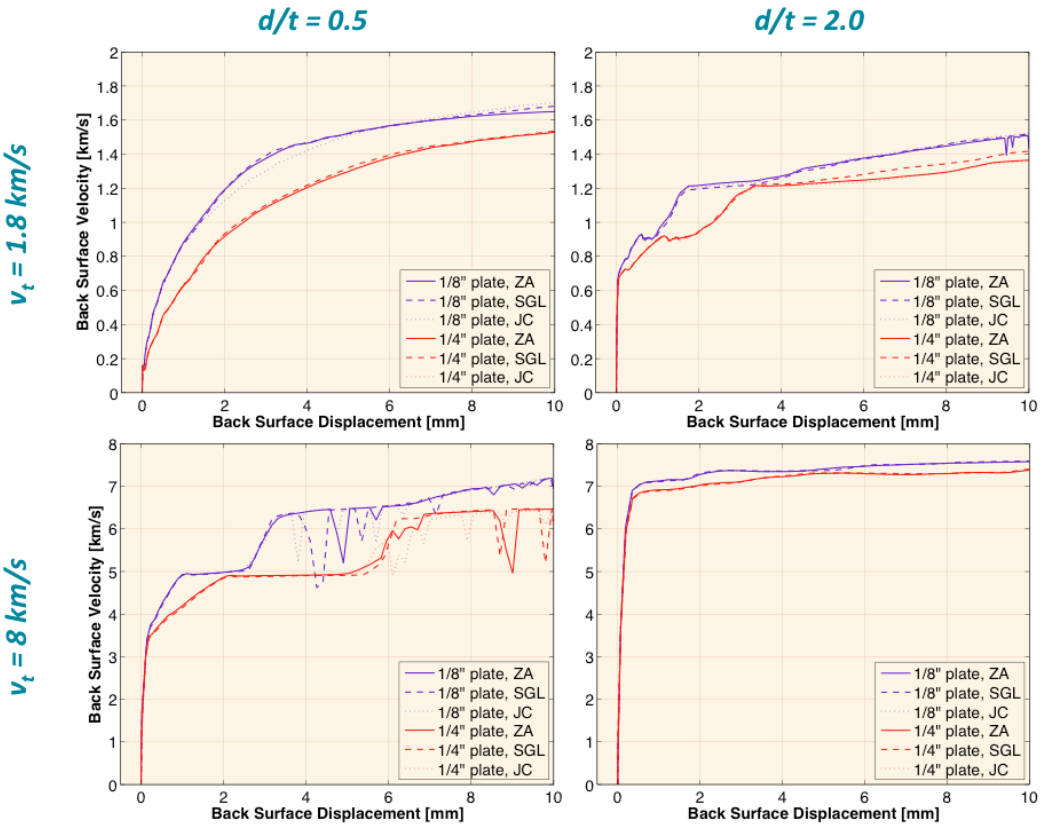

Fig. C-4 JC, ZA, and SGL strength models for Cu

List of Symbols, Abbreviations, and Acronyms

EOS	equation of state
JC	Johnson-Cook
MG	Mie-Grüneisen
RHA	rolled homogeneous armor
SGL	Steinberg-Guinan-Lund
ZA	Zerilli-Armstrong

1 (PDF) DEFENSE TECHNICAL INFORMATION CTR DTIC OCA

2 (PDF) DIRECTOR US ARMY RESEARCH LAB RDRL CIO LL IMAL HRA MAIL & RECORDS MGMT

1 (PDF) GOVT PRINTG OFC A MALHOTRA

3 (PDF) NAVSEA DAHLGREN W CHEPREN C DYKA M HOPSON

6 (PDF) SANDIA NATIONAL LABORATORIES K COCHRANE D LABRECHE J NIEDERHAUS S PETNEY E STRACK J SANCHEZ

2 (PDF) DSTL A MEARNS J CORDELL

1 (PDF) INL J LACY

1 (PDF) SURVICE ENGINEERING B BRUCHEY

34 (PDF) DIR USARL
RDRL CIH S
J CAZAMIAS
RDRL WML H
B AYDELOTTE
D MALLICK
C MEYER
D SCHEFFLER
B SCHUSTER
RDRL WMM B
B LOVE
RDRL WMP A
S BILYK
M COPPINGER
A PORWITZKY
C UHLIG
RDRL WMP C
R BECKER
T BJERKE
B LEAVY
S SEGLETES
RDRL WMP D
A BARD
W CLARK
M KEELE
D KLEPONIS
H MEYER
F MURPHY
C RANDOW
J RUNYEON
B SCOTT
K STOFFEL
G VUNNI
V WAGONER
M ZELLNER
RDRL WMP E
B CHAMISH
D HORNBAKER
J HOUSKAMP
T JONES
RDRL WMP G
R BANTON
J STEWART